Smart Network Control with Coordinated PV Infeed

Sabrina Hempel, Carl Schweinsberg, Jan-David Schmidt,
Dr.-Ing. Eckehard Tröster and Dr. Dipl.-Ing. Thomas Ackermann
Energynautics GmbH
Darmstadt, Germany
Email: s.hempel@energynautics.com

***Abstract*—The increasing amount of photovoltaic plants leads to voltage rise in the distribution grid. The standard control strategy of photovoltaic battery systems is aimed at maximizing the operators self-consumption. Instead of only optimizing the self-consumption, the battery can be operated in a grid-friendly manner, which relieves the grid. In addition, photovoltaic and battery inverter can reduce the voltage even more by providing reactive power. This paper presents a voltage regulation tool, which controls the active and reactive power of photovoltaic battery systems. The target of the active power control is to postpone the battery charging during the daily photovoltaic infeed peak (peak shaving). For this purpose, a simple prognosis model in combination with an adjustment control is evolved. The reactive power control is based on a voltage dependent reactive power curve which is parameterized in dependence of the position in the grid. This leads to a coordinated behaviour of all inverters in a distribution grid and ensures that all inverters provide a similar amount of reactive power. Moreover, the regulation tool notices if the grid topology has changed and adapts the reactive power control to this change.**

I. Introduction

In 2016, 1.5 GW of new photovoltaic (PV) plants were installed in Germany. Although this corresponds to 2 % of the worldwide installations, the goal of the German federal government was not achieved. In 2014, the German Renewable Energies Act (EEG) sets the goal of a yearly increase of installed PV power of 2.5 GW [1]. Thus, a further growth is to be expected.

98 % of all PV plants in Germany are connected to the low voltage distribution grid [1]. Already today, the increasing power in-feed of PV plants into the distribution grid leads to a considerable voltage rise. According to the German DIN EN 50160 norm, the voltage in the low distribution grid has to be within the boundaries of ± 10 % of the nominal voltage [2]. Thus, it is necessary to reduce the voltage in order to enable a further integration of PV plants into the distribution grid.

Within the framework of the project SNOOPI (Smart Network Control with Coordinated PV Infeed), new regulation tools are developed to maintain voltage stability and comply with set boundaries. The voltage regulation tool based on an active and reactive power control is designed to be scalable and transferable and can be applied to all distribution systems with high PV infeed paving the way for an even higher penetration of PV.

This paper is structured as follows: First, the background and the main goal of the project are described, and an overview of the project course is given. In the following two sections the active and reactive power control is described. Results and the impact of the regulation tool are presented in section five. The paper is concluded by an outlook.

II. Background and Main Goal

The increasing amount of PV plants in distribution grids leads to an inverse load flow and a voltage rise along the feeder at times with high PV generation. This situation is shown in Fig. 12, where P_G is the active power fed-in by the distributed generation (DG). In order to optimize the operator's self-consumption, most PV systems are connected to a battery. As the battery is often fully charged before midday, the PV peak is fed into the grid. By charging PV batteries in a grid-friendly manner, the voltage in the distribution grid can be reduced. In addition, PV and battery inverter can reduce the voltage even more by providing reactive power Q_G. Thus, battery systems can contribute to an increased amount of PV plants without the necessity of grid reinforcements.

The main goal of the project SNOOPI is to develop an autonomous and transferable SNOOPI-Box controlling PV and battery inverter. Autonomous because the box works independently without communicating with other boxes or devices. Only violations of voltage limits are reported to the DSO. Without any communication or configuration the SNOOPI-Box learns its position in the grid. Depending on its position, the reactive power control is adjusted. Thus, inverters located at the beginning of a feeder contribute in reducing the voltage as much as inverters at the end of a feeder although they register smaller voltages as can be seen in Fig. 12. Even if the topology of the grid changes, the algorithm adapts autonomously to this change.

The SNOOPI-Box is transferable because it is applicable to almost any arbitrary PV or battery inverter. This is achieved by using a SunSpec protocol enabling an interaction

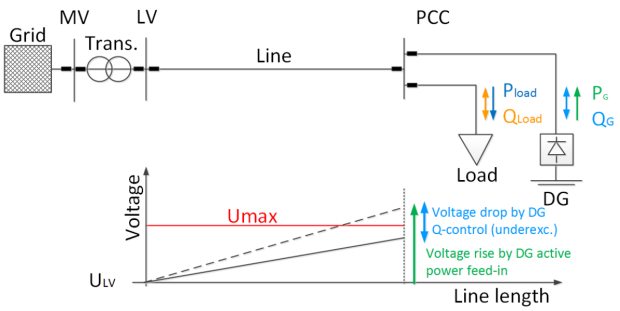

Fig. 1. Impact of active and reactive power on the voltage. [3]

with all compliant devices of members and partners of the SunSpec Alliance. Among them are the worlds leading manufacturers of inverters: SMA, Huawei, SolarEdge, Sungrow, ABB, Fronius and many others.

For developing and testing the SNOOPI-Box in a real distribution grid, a field test area in the network area of the German DSO EWR has been selected. The field test area is a rural area with high PV penetration. A large wind power plant is connected in the overlaying medium voltage feeder, leading to potentially high voltages at the distribution transformer. Therefore, the remaining allowed voltage rise becomes significantly smaller during times of high wind infeed. Seven battery systems equipped with a SNOOPI-Box will be installed in the distribution grid of the field test area. Although the algorithm is also applicable to PV inverters, the tests focus initially on battery inverters. The battery systems consist of a lithium-ion battery, a battery inverter and a smart meter provided by Fronius.

The first step was to build a simulation model of the grid of the field test area in DIgSILENT PowerFactory including loads, battery systems and PV infeed. The simulation model has been verified by measurements of phasor measurement units (PMUs). Besides testing the control algorithm in the simulation model, different switching states and different locations of the seven battery systems were investigated.

After the successful test of the control algorithm in the simulation model, the tool was tested in a laboratory setup consisting of a battery and an inverter. The reactive power control by the inverter and the communication between the voltage regulation tool and the inverter have been tested thoroughly. A user-interface was developed based on a web-browser application allowing the change of variables and visualization of measurement data such as voltage, active and reactive power while the control algorithm is running.

In the final step of the project, the field test will be carried out. In order to analyze the impact of the SNOOPI-Boxes in a distribution grid with high voltages, a switching state resulting in a long feeder and maximum voltages around 1.05 p.u. has been chosen. The seven battery systems are located along or close to this feeder. Thus, the behavior of SNOOPI-Boxes at different positions can be analyzed.

III. Active Power Control

A. Charging Strategy

The standard control strategy for PV battery systems is aimed at storing as much PV power as possible during a day. Therefore, the battery system is charged as soon as the PV power exceeds the load. As Fig. 2 displays, an economically sized battery system often reaches its maximum state of charge (SOC) already before noon and thus, before the PV peak. Consequently, the subsequent PV peak is supplied fully to the grid which leads to overcharge or loss of electricity production due to down-control by the DSO.

The sudden increase of active power in Fig. 2 can vary depending on the battery's capacity, which is presented through the arrow. The standard control strategy only intends to increase the PV system operator's self-consumption and energy autarky. Especially during summertime, the standard control strategy can be critical for the grid stability since the

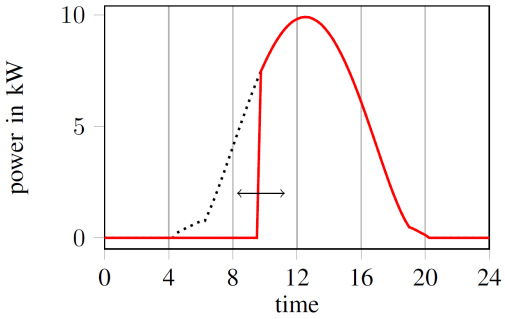

Fig. 2. Standard control strategy of a PV battery system for one day.

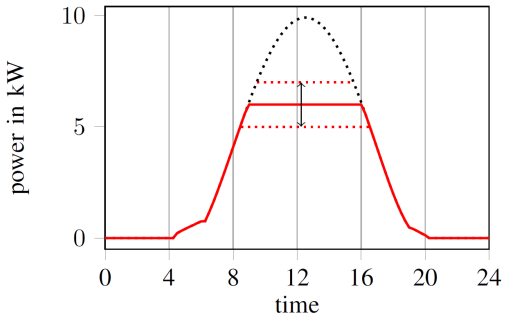

Fig. 3. Control strategy based upon a day-ahead prediction.

total PV generation is usually much higher as during wintertime. Thus, the grid has to be dimensioned for the 'Worst Case' scenario of PV in-feed although battery systems are existent [4].

In order to limit the critical PV peak infeed by using battery systems and simultaneously achieve a self-consumption which is comparable to the standard control strategy, a time displacement of the battery charging into the peak of the PV infeed is necessary. This is called 'peak-shaving' and is exemplified in Fig. 3. The active power plateau in Fig. 3 displays the power limit at which the PV generation is supposed to be capped. Based on the available battery capacity, the power limit is adjusted up- or downwards. The energy below the limit is supplied to the grid whereas the energy above is stored in the battery system. To achieve a high self-consumption and maximum limitation of the PV infeed, the whole battery capacity has to be used during the time of maximum PV infeed. Therefore, the PV generation and load situation has to be predicted upfront to hold battery capacity available during peak times. The target of the developed control strategy is to be grid-friendly as well as achieving a high self-consumption because of economical interests. For this reason, a control strategy is developed which is based on a prediction of the daily PV infeed.

The developed control strategy is based on a peak-shaving implementation which minimizes the PV infeed by using the whole battery capacity. For the following estimations, the underlying PV generation profile is determined based on local clear sky irradiance data with a resolution of 15 minutes provided by the database of Photovoltaic Geographical Information System (PVGIS) [5]. Fig. 4 shows the PV profile which is scaled to a rated power of 6 kWp. The curtailed PV peak (gray area) is identical to the assumed battery capacity of 5 kWh. The area below the power limit of 4.5kW equates

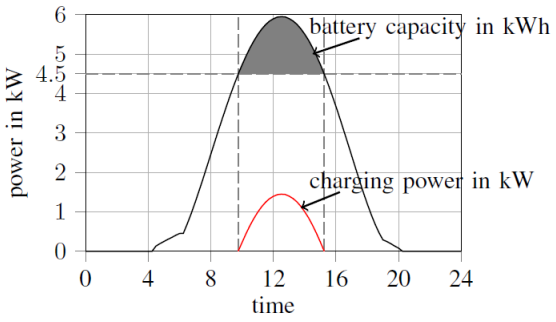

Fig. 4. Exemplary PV generation profile with a rated power of 6 kWp in combination with a battery capacity of 5 kWh.

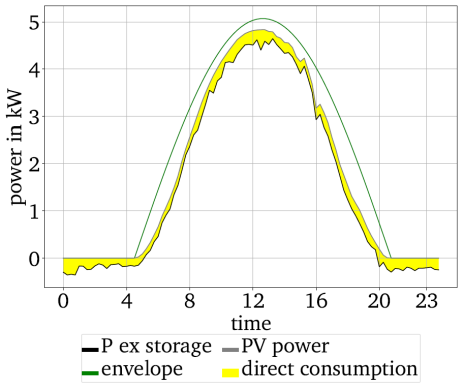

Fig. 5. Presentation of the generated envelope $f(x)$ for an exemplary day.

to the energy which is injected into the grid.

B. Prognosis Model

For limiting the local PV infeed at its best, the battery charging power has to be determined in advance. Therefore, the PV infeed needs to be predicted by means of a prognosis model. To keep it simple, the developed model is aimed at predicting an envelope of the actual daily PV generation. The envelope is based on the positive sine halfwave, which emulates a typical clear-sky PV generation profile fairly good. Due to the usage of the sine wave, the predicted values are reduced to three relevant values:

1) the PV generation maxima ($P_{PV,max}$),
2) the time of sunrise ($P_{PV} > 0$),
3) the time of sunset ($P_{PV} = 0$).

By means of equation (1), the daily envelope $f(x)$ is calculated in which the variable specifies the time from sunrise to sunset in minutes.

$$f(x) = P_{PV,max} \cdot \sin\left(\frac{\pi \cdot x}{\Delta t}\right) \text{ with } \Delta t = t_{PV=0} - t_{PV>0} \quad (1)$$

Fig. 5 illustrates an exemplary result of the daily prediction based on the developed prognosis model. The step size of the measurement is set to 15 minutes for all simulations executed in the course of this paper. This is chosen due to the amount of data generated and the run-time of the simulations.

The following examinations are based on a real PV generation profile of a PV system with a rated power of $P_r = 340$ kW. The PV system is located in the area of Darmstadt and has an orientation in south-east direction. It is measured over a period of one year with a step size of 15 minutes. The PV power output is assumed to be 1 kW/kWp. For the development of the prognosis model, the profile is scaled to a rated power of 6 kWp.

1) Usage of the Rolling Average Method for Predictions: As a first approach for the prognosis model, the rolling average method is used, which is a statistical tool for filtering time series. A series of averages is created from different subsets of the full dataset (time series). These averages generate a new filtered time series based on the previous one. The dimension of a subset is defined by a fixed window size of days or hours dependent on the resolution of the time series. The calculated average can be used as prediction for the next value.

Initially, the respective PV generation profile is prepared so that the three relevant values are extracted from the yearly

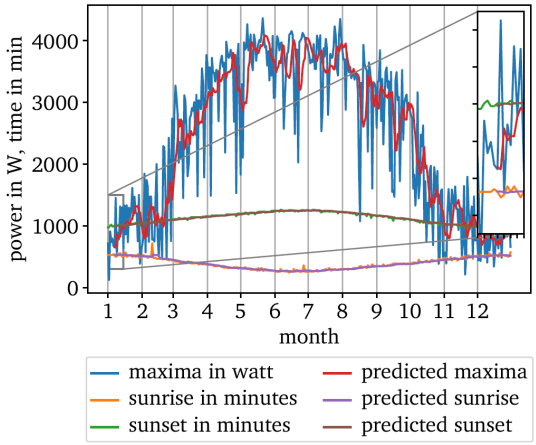

Fig. 6. Results of the predictions by using a rolling average with a window size of 6 days.

profile. Based on the mean squared error (MSE), which is a measure of the quality of an estimator, an optimal window size of six days is determined for the prediction of the three values. Fig. 6 compares the measured values with the predicted values of the maxima in watt, the sunrise and the sunset in minutes.

The daily predictions for sunrise and sunset are fairly good as the values show only a marginal scattering in the course of one year. On the contrary, the daily PV maxima are not adequately predicted as the comparison between predicted and measured PV maxima shows. For most of the days during a year, the predicted maxima are located below the measured ones. Additionally, days with a proportionally bad PV return due to bad weather have a strong influence on the predictions. Thus, the prognosis model has to be improved in terms of predicting the daily PV maxima.

2) Improvement of the Prognosis Model: The goal is to completely enclose the daily PV generation with the envelope $f(x)$ which is calculated using the predicted values. Therefore, the prognosis model is adapted to the requirements by setting boundaries to the day-to-day changes of the predicted PV maxima. On the one hand, a lower boundary is implemented based on the maximal gradient of the sine wave which patterns the yearly PV generation profile. Thus, the day-to-day change of the predicted maxima is bounded below by the determined maximal gradient which is set to 0,0075 kW/kWp in the developed control strategy. On the

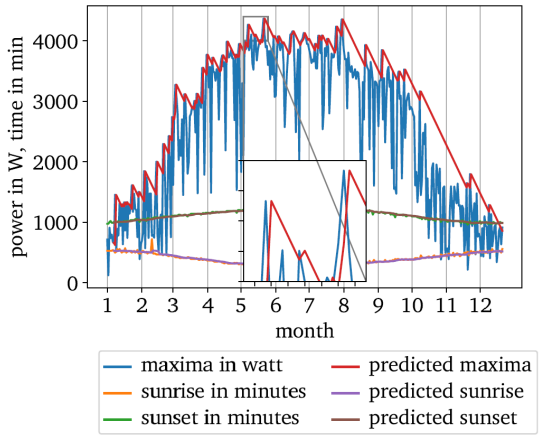

Fig. 7. Results of the predictions by using a rolling average with a window size of 6 days and including a lower and upper boundary.

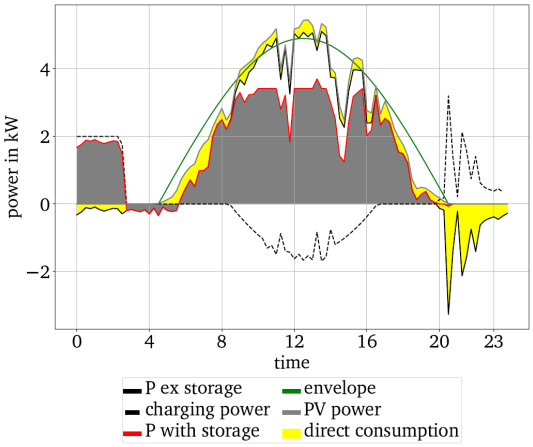

Fig. 8. Exemplary day for illustrating the adjustment control.

other hand, an upper boundary is implemented based on the persistence which is a forecasting method for weather predictions. The assumption is that the next value is identical with the preceding one. Within the control strategy, the predicted PV maxima for the next day is adjusted to the measured PV maxima of a day in case the predicted maxima is less than the measured one. Fig. 7 shows the final result of the developed prognosis model.

As can be seen, the predicted PV maxima lie above the measured maxima for the most days. Furthermore, the gradient is visible which bounds the day-today changes below. Since the prognosis model aims to calculate an envelope $f(x)$ which encloses the measured daily PV infeed, this result is as desired.

C. Adjustment Control

Based on the predicted envelope $f(x)$, the battery charging power $P_{Bat,pred}$ is predicted for each time step of a day as it is already explained in section III-A. In order to adapt the predicted values to the measured ones during the day, an adjustment control is integrated in the control strategy. The target of the control is to keep the PV infeed at the limit which results by charging the battery system during PV peak by means of the predicted charging power (see Fig. 4). Depending on the predominant situation per time step, the predicted battery charging power is either increased or decreased through the adjustment control or remains unchanged. Fig. 8 illustrates an exemplary day.

Between 8 and 12 o'clock as well as between 12 and 16 o'clock in Fig 2, the charging power (dashed line) is increased in some time steps (each is 15 minutes). During these time steps, more energy is saved in the battery than was restrained for those particular steps. To prevent the battery from reaching its maximum SOC before the PV peak is perfectly limited, the charging power has to be reduced in a next time step in case the predominant in-feed situation allows it. This happens at about 11 o'clock and 15 o'clock respectively when the PV in-feed falls below the envelope.

If, in contrast, the charging power is decreased during a time step because of battery discharging during the day when load exceeds PV generation, it has to be increased in a next one. Thus, the adjustment control reacts to the PV in-feed situation in each time step for best possible limiting the PV peak by using the predicted battery charging power. For this purpose the actual SOC is constantly compared to the provided SOC. If there is a (positive or negative) difference between both SOCs due to an increase or decrease of the predicted battery charging power during a time step, the charging power is adjusted as follows:

$$P_{adjust}(t) = P_{opt}(t) + (\mathrm{SOC}_{opt}(t) - \mathrm{SOC}_{akt}(t)) \cdot \frac{60}{\Delta t}. \quad (2)$$

IV. Reactive Power Control

A. Voltage Regulation

The reactive power setpoints are determined using an autonomously parameterized $Q(U)$ characteristic curve, where Q is the reactive power and U the voltage. The parameterization ensures a coordinated behavior of all inverters. In Fig. 9 the $Q(U)$ curve is displayed. Q_{min} and Q_{max} are the minimum and maximum reactive power which can be provided by the inverter. These limits are specified by the the inverters capability curve or limits imposed by the manufacturer.

The values U_3 and U_4 of the $Q(U)$ curve depend on the maximum voltage U_{max} measured at the connection point:

$$U_3 = U_N + 0.5 \cdot (U_{max} - U_N), \quad U_4 = U_{max}, \quad (3)$$

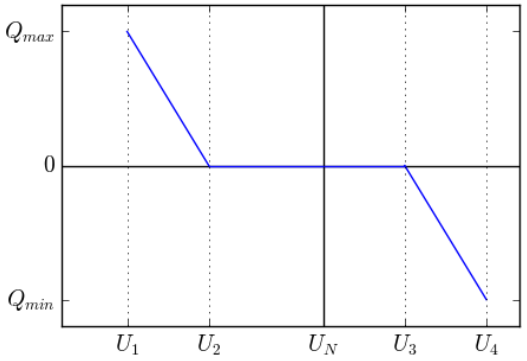

Fig. 9. $Q(U)$ characteristic curve.

where U_N is the nominal voltage. Thus, the inverter starts to provide reactive power if the voltage reaches 50% of the maximum voltage excess. At a voltage which equals the maximum measured voltage U_{max}, the reactive power is at its maximum. The value U_1 is given by the minimum measured voltage U_{min}. As the characteristic curve should be symmetric due to the location of the inverter, U_2 is determined by the slope between U_3 and U_4, thus:

$$U_1 = U_{min}; \quad U_2 = U_{min} + 0.5 \cdot (U_{max} - U_N)\,. \qquad (4)$$

Due to the increase of the maximum voltage along a feeder, the maximum voltages at inverters at the beginning of a feeder are smaller. The dependency of the starting point U_3 on U_{max} ensures that all inverters along a feeder will start to provide reactive power at the same time.

The voltage change caused by the reactive power depends on the reactance of the cable. Simplified this can be expressed as follows [6]:

$$dU \approx \frac{RP + XQ}{U_N^2}. \qquad (5)$$

Here, dU is the voltage change, R the resistance, X the reactance, P and Q the active and reactive power, and U_N the nominal voltage. In a distribution grid, the relation R/X is generally larger than 1. Thus, the active power has a larger influence on the voltage than the reactive power. Both, the resistance and the reactance increase proportionally with the length of the cable. As a result, inverters at the beginning of a feeder have a smaller influence on the voltage than inverters at the end of a feeder when providing the same amount of reactive power.

The above parameterization also specifies the slope of the $Q(U)$ curve in dependence of the position in the grid: The smaller the maximum voltage, the smaller is the influence of the inverters and the steeper is the slope. The maximum allowable slope with regard to the stability of the $Q(U)$ control was discussed, amongst others, in [7] and [8].

In [7] a slope of 11 $\%_{Q_{max}}/V$ is recommended which corresponds to an reactive power increase from 0 to Q_{max} within 2.3 % of the nominal voltage. This value was received for inverters at a low voltage feeder under extreme conditions. A reactive power increase within 1 % of the nominal voltage (25 $\%_{Q_{max}}/V$) violates only one stability criterion in most cases. In [8] all tested parameterizations resulted in a stable behavior of the inverter. The steepest parameterization investigated was a reactive power increase from 0 to Q_{max} within 1 % of the nominal voltage. The parameterization in (3) and (4) was chosen such that, in most cases, the reactive power increases from 0 to Q_{max} within a voltage change larger than 1 %. If the $Q(U)$ characteristic curve is steeper, the value U_1 is decreased and U_4 is increased in order to maintain stability.

B. Learning Mechanism

The SNOOPI-Box adjusts the reactive power control autonomously. As described in the previous section, this is achieved by the dependence of the $Q(U)$ characteristic curve on the maximum voltage. The maximum voltage is determined easily by the measurement of the voltage. Depending on the weather and the season when the SNOOPI-Box is installed, it can take several month until the maximum voltage reaches its highest value.

The more difficult task is to realize a change of the grid topology. If a switching in the distribution grid changes the position of the SNOOPI-Box from the beginning of the feeder to the end of the feeder, the voltage at the inverter will increase. In this case, the SNOOPI-Box will adapt the maximum voltage without the need for further functions. In the reverse case however, i.e. the position of the SNOOPI-Box is changed from the end of the feeder to the beginning of the feeder, the voltage at the inverter decreases. Without further functions, the maximum voltage will remain at its high level. This problem is solved by determining the influence of the reactive power on the voltage.

As explained in the previous section, the reactance X increases proportionally with the line length. Thus, reactive power provided at the beginning of the line will have less influence on the voltage than reactive power provided at the end of a line. The SNOOPI-Box uses this effect in order to notice a change in the grid topology.

In order to determine the influence of the reactive power on the voltage, the SNOOPI-Box periodically performs a calibration: Different reactive power setpoints are passed to the inverter and the change of the voltage is measured. The influence of the reactive power on the voltage is determined by dividing the voltage change dU by the reactive power change dQ. To filter other influences out of this value, the influence of the reactive power is calculated multiple times and the results are evaluated statistically.

V. Simulation Results of the Active Power Control

In the following two sections simulations results of the active and reactive power control are presented. Both control algorithm have been tested separately. One of the next steps is to combine the active and reactive power control and test the combination in a simulation model.

The active power control strategy is simulated in a grid model consistent of a single branch line to which 15 terminals are connected. Each terminal consists of a PV battery system and a load. Each PV system has the same PV generation profile which is based on the already introduced profile from section III-B. The certain load profiles are taken from a survey of the 'Hochschule für Technik und Wirtschaft' in Berlin [9] and represent real profiles of single households. The following examinations refer to terminal 15 at the very end of the branch line for which the yearly electricity demand is about 3.8 MWh and the yearly peak power is 18.61 kW. The ratio of PV rated power and battery capacity are equal for each terminal per simulation run.

Both, PV rated power and battery capacity, are varied with a step size of 2 in the range of 4 kWp to12 kWp for the rated power respectively 4 kWh to 12 kWh for the battery capacity. Per constellation, a simulation run is executed in PowerFactory with a horizon of one year in 15 minute time steps.

A comparison of the following control strategies is conducted:

- *strategy 1* which equates to the developed control strategy based on the prognosis model (see section III-B),

- *strategy 2* which equates to todays standard control strategy for PV battery systems, which is solely used for maximizing the PV system operators self consumption (see section III-A),
- *strategy 3* which is based on a perfect forecast of both, the generation and load situation of the next day and therefore represents the optimal case.

Based on preliminary examinations, a daily discharge of each battery system is assumed in the executed simulations. Priority objective is to achieve the daily battery discharge through the electricity demand of the respective household. If the demand is not sufficient, the battery system is forced to discharge during the night. Thus, the entire battery capacity is available every day to limit the daily PV infeed. In reality, this may be implemented by adjusting the load by means of electrical vehicles or heat pumps. Furthermore, the battery systems depth of discharge (DoD) is limited to 80 %. In reality, this is a common assumption to extent the life span of a battery system. The efficiency of the battery system is moreover assumed to be 100 %.

The developed control strategy (strategy 1) is compared to the two other strategies (strategy 2 and 3) on the basis of the annual average self-consumption (equation (6)) as energetic assessment criterion as well as the ability for reducing the PV infeed as assessment criterion for the grid-friendly behaviour of strategy 1:

$$e = \frac{\sum P_{DC} \cdot \Delta t + \sum P_{BC} \cdot \Delta t}{\sum P_{PV} \cdot \Delta t}. \tag{6}$$

Here, P_{DC} is the direct consumption of the PV generation for feeding the electricity demand of the household, P_{BC} is the battery charging power and P_{PV} is the PV power generation.

A. Energetic Comparison

All the results which are discussed in the following are calculated on the basis of computational simulations with the previously made assumptions. Initially, the annual average self-consumption is examined. Fig. 10 compares strategy 1 with strategy 2. Shown is the annual average self consumption for an increasing PV rated power. Each color represents a different battery capacity. The yellow area describes the direct consumption which is equal for each battery capacity since the PV and load profile is equal from case to case.

As can be seen, the annual average self consumption decreases with an increasing PV rated power since a larger daily PV excess power is produced. Increased battery capacity, meanwhile, results in a higher share of annual self-consumption due to enhanced flexibility to store PV excess energy. Since it is assumed that the battery system is entirely discharged every day, the self consumption increases continuously with rising battery capacity as no limiting effect is occurring due to not entirely discharged battery systems. By looking at Fig. 10, a slightly higher annual average self consumption is visible for strategy 2 compared to strategy 1. This means, using strategy 2 results in more total energy stored during a year than using strategy 1. However, the difference for each constellation of PV rated power and battery capacity is small. On average, strategy 1, which equates to the developed control strategy, is 0.72 % worse than strategy 2, which equates to the standard control strategy. The largest difference is recorded for the constellation of 4 kWp PV rated power and 12 kWh battery capacity with a values of 1.73 %. This percentage difference equates to an energetic difference of 62 kWh per year.

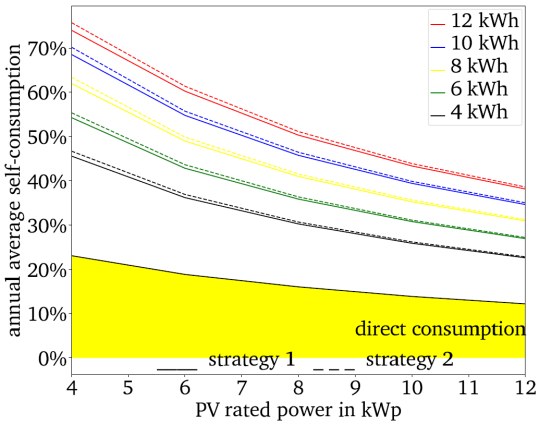

Fig. 10. Comparison of the annual average self consumption of strategy 1 (solid lines) and strategy 2 (dashed lines).

B. Comparison of the PV Peaks

There is no difference between strategy 2 and strategy 3 in terms of energetic aspects. Thus, the comparison between strategy 1 and strategy 3 is negligible. In the following, strategy 1 is compared to both of the other strategies regarding the measured infeed peak.

Fig. 11 compares strategy 1 with strategy 2 and strategy 3. Generally, with an increasing PV rated power the PV infeed maxima increase also per battery capacity. Regarding strategy 2, despite having battery systems connected to the grid, the PV infeed maxima remain constant. Thus, the standard control strategy does not lead to a reduction of the grid load as the PV system still injects its peak power into the grid. However, with strategy 1 a significant decrease of the PV infeed maxima is visible which increases with decreasing battery capacity. The increase of the PV infeed maxima for a PV rated power of 4 kWp and battery capacities of respectively 10 and 12 kWh occurs due to the implemented battery discharging over night which exceeds the PV infeed maximum in this case. On average, the PV infeed maximum can be reduced around 23 % compared to strategy 2.

The perfect foresight model represents the optimal case and therefore, the comparison between strategy 1 and strategy 3 identifies the potential of a control strategy which is based on a PV infeed prediction for the next day. As visible in figure 12, strategy 3 runs below strategy 1 for every constellation of PV rated power and battery capacity (difference between solid and dashed lines). Thus, an even better result is achievable with a more accurate prognosis model. The average difference between the PV infeed maxima of strategy 1 and strategy 3 is of around 12 %.

To conclude, strategy 1 mitigates the PV maxima 23 % on average compared to strategy 2 and strategy 3 mitigates them 12 % on average compared to strategy 1. In other words, strategy 1 based on a simple prognosis model is two thirds as effective as strategy 3 which is based on perfect foresight.

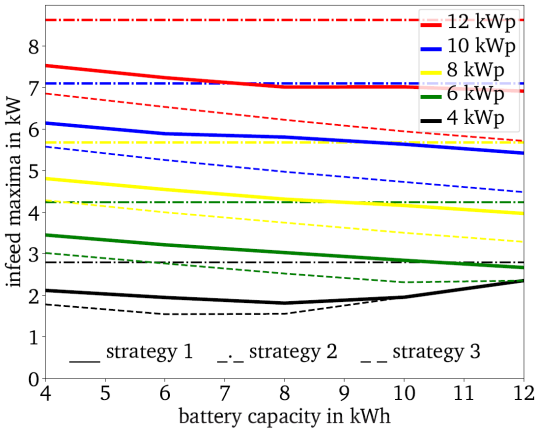

Fig. 11. Comparison of the PV infeed maxima of strategy 1 (solid lines) and strategy 2 (dash-dotted lines) and strategy 3 (dashed lines).

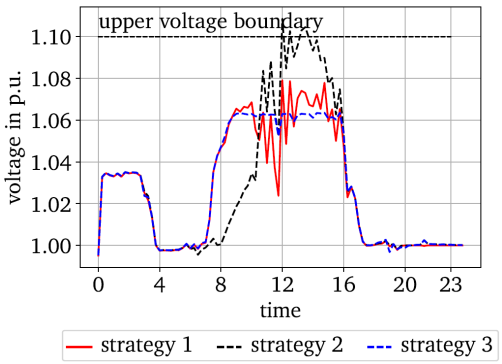

Fig. 12. Comparison of the voltage run of an exemplary day for the three strategies.

C. Examination of the Votlage

Fig. 12 exemplary shows the voltage across the branch line of the grid model for a ratio of PV rated power and battery capacity of 1 kWh/kWp. The considered terminal is terminal 15 at the very end of the branch line. By applying strategy 2, the upper voltage boundary is violated at this particular day whereas with both of the other strategies the voltage stays within the mandatory boundaries of 0.9 to 1.1 p.u. related to the nominal grid voltage. Compared to strategy 2, the voltage peak is reduced by 3 % with strategy 1 (from 1.109 p.u. to 1.079 p.u.) and is reduced by 4 % with strategy 3 (from 1.109 p.u. to 1.064 p.u.). Due to perfect knowledge of the infeed situation, the voltage can be kept on an almost constant limit by means of strategy 3. However, the voltage scatters around a certain voltage limit by applying strategy 1 since battery charging power is calculated on the basis of the envelope which equates to a clear-sky PV profile.

VI. Simulation Results of the Reactive Power Control

The reactive power control was simulated in a DIgSILENT PowerFactory model based on real PV data and load profiles. Fig. 13 shows a map of the field test area. The green letters indicate the positions of the battery systems in the real distribution grid and in the simulation model. Most battery systems are located at a long feeder (illustrated in blue) with voltages between 0.93 p.u. and 1.06 p.u.. All simulation results presented in this paper are based on a step size of one minute, i.e. every minute the inverter measures the voltage and passes the value to the SNOOPI-Box. The SNOOPI-Box passes a reactive power setpoint dependent on this voltage to the inverter.

In section VI-A and VI-B a whole year was simulated and the coordination of the battery systems are examined. In section VI-C the behaviour of the regulation tool is investigated in the case of a grid switching. For this purpose, only the time before and after the switching is relevant, which is why only two months were simulated.

A. Learning Behaviour

In Fig. 14 the influence of the reactive power on the voltage dU/dQ is plotted at the top, and the maximum measured voltage U_{max} is plotted at the bottom for all battery systems. The different battery systems can be distinguished by the color.

In the first night of every month the influence of the reactive power on the voltage is determined by the calibration. Due to the calibration, dU/dQ changes slightly every month which is caused by other influences on the voltage which could not be filtered out completely. Between the calibrations, the influence can also change by determining the reactive power and voltage change during the normal reactive power control.

In the considered distribution grid, the influence of reactive power on the voltage is quite small. As was to be expected, the battery system D, which is positioned at the end of the feeder, has the largest influence on the voltage. If the inverter D provides the minimum reactive power of -53 %, the voltage is reduced by 0.32 % points. The system E is placed closer to the distribution transformer and thus, has an even smaller influence.

The results prove the importance of a coordinated behaviour of the battery inverter. If the inverter closer to the distribution transformer wouldn't contribute to reduce the voltage to the same extent, the influence on the voltage

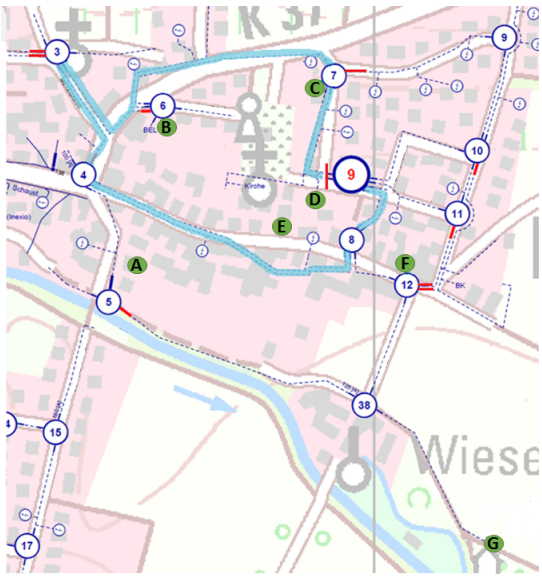

Fig. 13. Map of the field test area. The green circles indicate the positions of the battery systems.

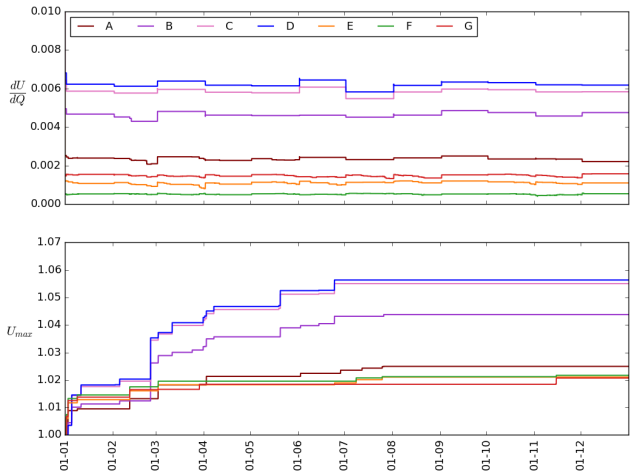

Fig. 14. Learning behaviour of all battery systems. Top: Influence of the reactive power on the voltage. Bottom: Maximum measured voltage.

would be insignificant. Moreover, the result shows that the value dU/dQ is a good indicator of a switching.

As can be seen in the lower figure, the order of the maximum measured voltage U_{max} of the different battery systems is similar to the influence as expected. In contrast to the influence however, which calibrates during the first night, the maximum voltage reaches its final value only in June on a sunny day with high PV in-feed. Before the maximum value is reached, the inverter will provide more reactive power than needed. But once the final value is adopted, the inverter will provide only reactive power when it is needed, i.e. mainly during the summer months as the PV in-feeds and thus the voltages are higher.

B. Q(U) Control

In dependence of the maximum voltage, the $Q(U)$ characteristic curve of the inverters are parameterized. Fig. 15 shows the different $Q(U)$ curves of three battery inverters at different positions. As can be seen, battery systems located closer to the distribution transformer have a smaller dead band and a steeper slope.

In Fig. 16 an example day of the voltage dependent reactive power control is shown which is based on the $Q(U)$ curve in Fig. 15. The 24th of June is the day with the maximum voltage which is plotted at the top. The bottom diagram shows the reactive power in-feed. Although the voltage at the battery B is smaller, the inverter provides almost the same amount of reactive power as the inverter D. The characteristic of the voltage at position E deviates from the other positions. The maximum voltage, for example, is not reached at 14:30 but at 17:00 o'clock. Therefore, the reactive power in-feed also deviates. But due to the parameterization all three inverters start and stop to provide reactive power at the same time. Moreover, they provide a similar amount of reactive power although the voltage levels are different.

Fig. 17 shows the Pearson correlation coefficient of the reactive power in-feed of all seven battery systems from the 1st of August to the 31st of December (after the maximum voltage at all battery systems has reached its highest value). The Pearson correlation coefficient is a measure of the linear

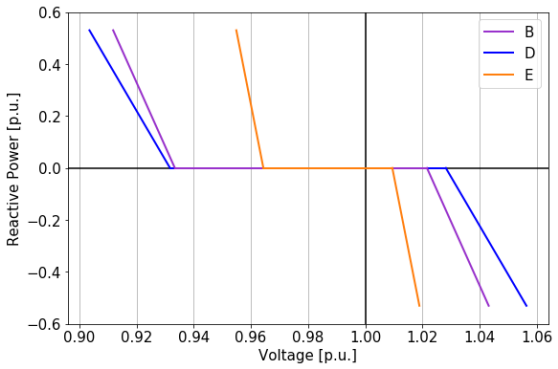

Fig. 15. Parameterized $Q(U)$ characteristic curve of three battery inverters at different positions.

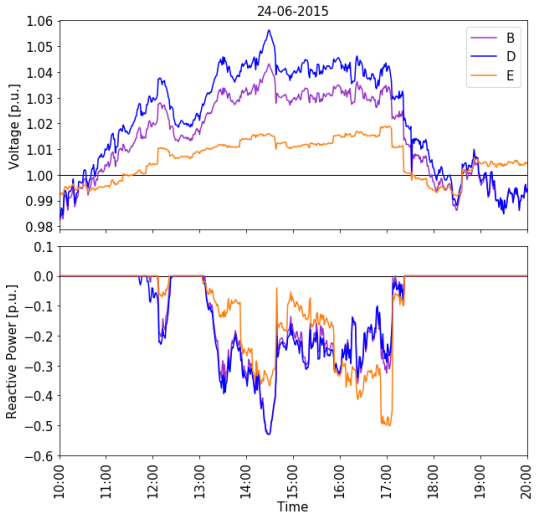

Fig. 16. Example day of the voltage depended reactive power control of three battery inverters at different positions. Top: Measured voltage. Bottom: Reactive power in-feed.

correlation between two variables. A coefficient between 0.1 and 0.3 indicates a small correlation, between 0.3 and 0.5 a moderate correlation and a coefficient larger than 0.5 indicates a strong correlation [10].

The reactive power in-feed of the battery systems A, B, C and D correlates strongly. The correlation between B, C and D even is very strong as all three have a correlation coefficient larger than 0.97. This has been observed also in Fig. 16 and is due to the positions of the battery systems at the end of the same feeder. The systems F and G correlate only little with B, C and D as they are not connected to the same feeder. Although the system E is connected to the same feeder, it correlates only moderately with the systems B, C and D. This can be explained by investigating the loads at the feeder between the places 8 and 4 which influence the voltage. Between the morning and the afternoon these loads often have high peaks whereas the loads at the end of the feeder are considerably smaller at these times. This is also the reason why the voltage peak between 14:00 and 15:00 o'clock in Fig. 16 can't be observed at the battery system E, which has a high load peak at that time.

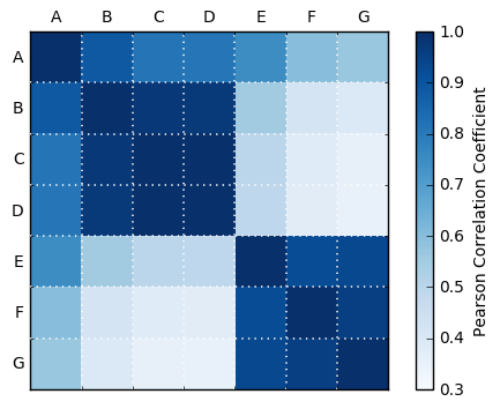

Fig. 17. Correlation of the reactive power in-feed of the different battery systems from the 1st of August to the 31st of December.

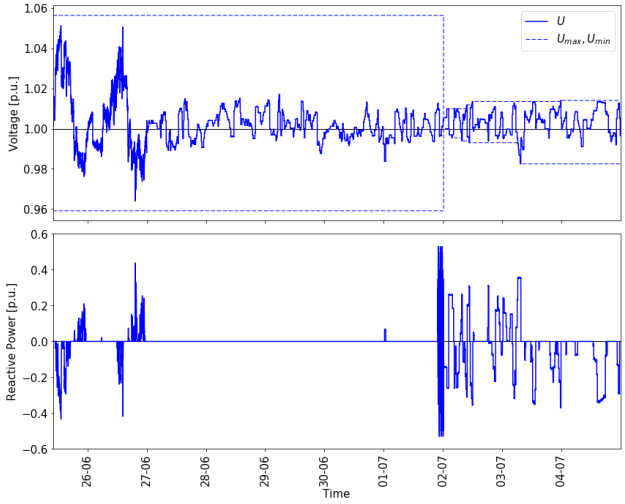

Fig. 18. Top: Measured voltage (solid line), and the maximum and minimum voltage (dashed lines) of the battery system D from the 25th of June to the 5th of July. Bottom: Reactive power in-feed of the battery system. On the 27th of June the grid is switched.

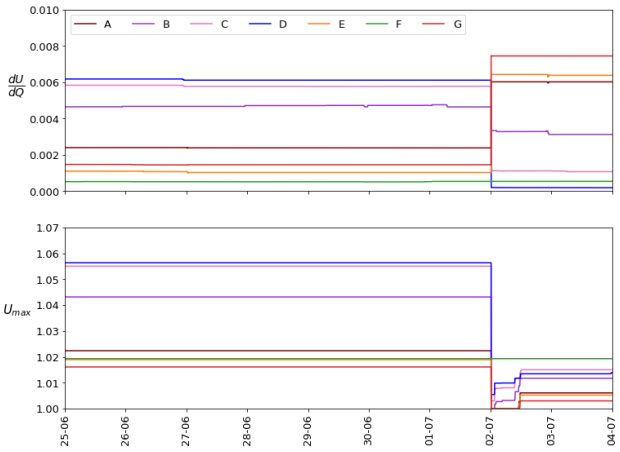

Fig. 19. Learning behaviour of all battery systems from the 25th of June to the 5th of July. On the 27th of June the grid is switched. Top: Influence of the reactive power on the voltage. Bottom: Maximum measured voltage.

C. Switching

The influence dU/dQ is determined in order to notice a change in the grid topology. In this section, the grid is switched during the simulation, so that the feeder is fed from the back. The months June and July were simulated and the switching was implemented on the 27th of June. After the switching, the battery system D is not placed at the end of the feeder but at the beginning.

At the top of Fig. 18 the voltage course and the maximum and minimum voltage at position D is shown from the 25th of June to the 5th of July. The reactive power in-feed is shown at the bottom. From the 27th of June, the voltage is much smaller due to the switching. As the maximum and minimum voltages remain on their high level for the rest of the month, the inverter provides almost no reactive power. In the first night of the month (02-07) the calibration is carried out and the influence on the voltage is determined. As can be seen at the top of Fig. 19, the influence dU/dQ of the battery system D drops considerably. As a result, the maximum and minimum voltages are determined newly and the $Q(U)$ control is adjusted to the new values.

Due to the switching, the battery systems B, C and D have a lower influence as before, while the influence of the systems A, E and G increases. Fig. 19 shows, that the maximum voltage of these battery systems is determined newly because the influence has changed. The position of the battery system F hasn't changed, as it is not connected to the same feeder, which is why the maximum voltage of this system is not determined newly.

VII. Conclusion and Outlook

In the course of this paper, an active control strategy for distributed PV battery systems has been developed which achieves an annual average self consumption comparable to the standard control strategy. The percentage difference amounts to under 1 % on average. At the same time, the PV infeed maximum can be reduced by around 23 % on average. This significantly contributes to a relief of the grid and thus reduces grid reinforcement and voltage issues. However, the achieved PV infeed maxima are in average 12 % higher compared to a control strategy based on perfect foresight. Still, this is a good result with respect to the simplicity of the implemented prognosis model in combination with the developed adjustment control. Nevertheless, further improvement is required concerning the prognosis model, e.g. on the basis of numeric weather models. Additionally, the developed control strategy should be examined in other grid topologies or with modified PV generation and load profiles.

By parameterizing the $Q(U)$ characteristic curve in dependence on the maximum measured voltage, all inverters in a distribution grid provide reactive power coordinately without communicating with each other. The advantage of a coordinated behaviour is that inverters placed at the beginning of a feeder also help to reduce the voltage although they don't measure high voltages. This is important as the influence of the reactive power on the voltage in distribution grids is often quite small.

In the following months the active and reactive power control will be combined and the interaction of both will be investigated. In addition, the field test will be carried out and initially the reactive power control of the SNOOPI-Box will be tested in a real system.

The final outcome of the project will be a device which

reduces the voltage considerably by controlling reactive and active power without impairing the system operator. As the SNOOPI-Box is applicable to almost any inverter and hardly any presettings are necessary, it is easy to install at many inverters in a distribution grid with voltage problems. Even if the status of the grid changes, for example if new PV plants are installed or by a switching, the SNOOPI-Box doesn't have to be reconfigured but adjusts its control autonomously. Furthermore, no communication infrastructure is necessary for operating the developed control strategy. Thus, it will pave the way for a high PV penetration.

REFERENCES

[1] H. Wirth, "Aktuelle Fakten zur Photovoltaik in Deutschland," 2017.

[2] T. Aundrup, H.-P. Beck, A. Becker, A. Berthold, and A. Conreder, "Batteriespeicher in der Nieder- und Mittelspannungsebene - Anwendungen und Wirtschaftlichkeit sowie Auswirkungen auf die elektrischen Netze," 2015.

[3] M. Kraiczy, L. Al Fakhri, T. Stetz, and M. Braun, "Do It Locally: Local Voltage Support by Distributed Generation - A Management Summary," 2017.

[4] G. Kerber, "Empfehlung zur Richtlinie zum Anschluss von Erzeugungsanlagen an das Niederspannungsnetz," 2015.

[5] E. Kommission, "Photovoltaic Geographical Information System (PVGIS)," 2015.

[6] L. Fickert, M. Sakulin, and W. Hipp, "Netzaspekte von dezentralen Erzeugungseinheiten - Studie im Auftrag der E-Control GmbH," 2004.

[7] M. Lindner, R. Witzman, O. Marggraf, S. Laudahn, B. Engel, S. Patzack, H. Vennegeerts, A. Moser, M. Gödde, F. Potratz, and A. Schnettler, "Ergebnisse der FNN-Studie zu neuen Verfahren der statischen Spannungshaltung ," 2014.

[8] C. Elbs, R. Nenning, R. Pardatscher, and R. Witzmann, "Einsatz der Q(U)-Regelung bei der Vorarlberger Energienetze GmbH," 2014.

[9] D. Tjaden, J. Bergner, J. Weniger, and V. Quaschning, "Repräsentative elektische Lastprofile für Wohngebäude in Deutschland auf 1-sekündiger Datenbasis." 2015.

[10] J. D. Chee, "Pearson's Product-Moment Correlation: Sample Analysis," 2015.